Electronic Supplementary Material (ESI) for ChemComm.

Electronic Supporting information (ESI)

For

Template-free Fabrication of Highly-Specific SERS Substrates by Co-precipitating Functional Nanomaterials during the Self-sedimentation of Silver Nanowires into Nanoporous Film

RuiLiu,[a] Jie-fang Sun,[a] Dong Cao,[a] Li-qiang Zhang,[b] Jing-fu Liu*[a] and Gui-bin Jiang[a]

a State Key Laboratory of Environmental Chemistry and Ecotoxicology, Research Center for Eco-Environmental Sciences,
Chinese Academy of Sciences, Beijing 100085, China.
b State Key Laboratory of Heavy Oil Processing and Department of Materials Science and Engineering,
China University of Petroleum, Beijing 102249, China

jfliu@rcees.ac.cn

Table of content

1. Materials and Chemicals.

p-Nitrothiophenol (p-NTP), Crystal Violet (CV), aflatoxins (AFTs B_1, B_2, G_1 and G_2), $FeCl_3$ were purchased from Sigma-Aldrich.2, 6-dimethylphenylisocyanide (2, 6-DMPI) was brought from Alfa Alser. Triton X-114 (TX-114) was brought from Acros Organics (Geel, Belgium). $AgNO_3$, $PdCl_2$ and NaCl were supplied by Sinopharm Chemical Reagent Co. (Beijing, China). KBH_4 was purchased from Jinke Chemical Research Institute (Tianjin, China). All the chemicals are at least analytic grade, and Milli-Q water was used throughout this study.

2. Experiment Section

2.1 Material synthesis

2.1.1 Synthesis of Ag NWs and Ag NPF.

Ag NWs were synthesized according to our previously reported procedure.[1] Briefly, under vigorous stirring, 3 mL ice-cooled 200 mM KBH_4 solution was quickly injected into a 47 mL ice-cooled aqueous solution containing 0.1mmol of $AgNO_3$ and 25 mg of TX-114, and the resulting solution was placed in a septum-sealed 50 mL flask. After the addition of KBH_4, the mixture was further stirred for 1 min at 0 ^oC. As substrate for the deposition of Ag NPF, silicon wafers (1 cm × 1 cm) were ultrasonically cleaned successively in 10 % HCl, ethanol, and water for 30 min each and then dried in air. The cleaned silicon wafers were placed on the bottom of a 24-well plate (or flat glass container), into which 2.8 mL of freshly prepared Ag NW solution/dispersion was added. The container was stored undisturbed at 4 ^oC for 12 h. After this, the upper colorless aqueous solution was removed carefully with a pipet, and the formed dark green gel-like thin layer was dried at 4 ^oC and 70% relative moisture and washed twice with cold ethanol.

2.1.2 Preparation of Ag NPF-γ-Fe_2O_3 NSs hybrid nanocomposite.

For the gifting of Ag NPF with Arsenic/Arsenite (As(III)/As(V)) ion capture functionality, a good As(III)/As(V) ion sorbent, *i.e.* γ-Fe_2O_3 NSs were in-situ synthesized and co-sediment with Ag NWs. Specifically, after the injection of KBH_4 into $AgNO_3$ solution, and stirring for 1 min, 5 mL 2.0 mM $FeCl_3$ was dropwisely added into Ag NWs dispersion under vigorous stirring. Again, the synthesized hybrid nanostructure was deposited on Si wafer.

2.1.3 Preparation of Ag@Pd NPFs.

To make Ag NPF catalytic active and Pd SERS active, Pd nanocatalyst, both in the form of Pd overlayer and Pd branches, were in-situ synthesized and co-sediment with Ag NWs.[2] Specifically, after the injection of KBH_4 into $AgNO_3$ solution, and stirring for 1 min, 1 mM Na_2PdCl_4 was dropwisely added the solution under vigorous stirring. The amount of added Pd is 0.25%, 0.50%, 1.0%, 2.0%, 4.0%, 6.0% and 8.0 % relative to that of Ag. Again, the synthesized hybrid nanostructure was transferred into a 24-well plate, where a 250 μm transparent SiO_2 wafer was already placed in. The container was stored undisturbed at 4 ^oC for 8 h. After that, the upper colorless aqueous solution was removed carefully with a pipet, and the formed black gel-like thin layer was dried at 4 ^oC and 70%

relative moisture and washed twice with cold ethanol.

2.2 SERS performance of Ag NPF.

The SERS activity of Ag NPF was testified from the viewpoint of large area uniformity and sensitivity. For the characterization of large area uniformity, Ag NPF was placed into 5 mL 10^{-8} M thiophenol (TP) ethanol solution for 5 min to loading a sub-monolayer of TP molecule on Ag surface. After washed with copious ethanol, SERS mapping were performed on a random selected 400μm × 400μm area with a step-size of 5 μm×5 μm, and a total of 6561 spectra were collected. The sensitivity of Ag NPF as SERS substrate was testified both by a comment Raman probe-CV and a non-resonance AFTs. For this purpose, 10 μL ethanol solution of CV and AFTs was loaded on Ag NPF. After air-dried, SERS spectra were excited by 633 nm Laser at low power density (less than 10^{7} mW cm^{-2}), the integration time was 5 second.

2.3 Ultra-sensitive SERS analysis of As(V) by Ag NPF-γ-Fe_2O_3 NSs.

For the analysis of As(V) ion, Ag NPF-γ-Fe_2O_3 NSs was placed into 5 ml As(V) with different initial concentration for 30 mins. After that, the As(V) ion captured Ag NPF-γ-Fe_2O_3 NSs was washed with water to remove unbounded As(V) ion. The ion interference experiments were performed in 7.5 μg L^{-1} or 0.1μM As(V) that coexisted with mM-level Na^{+}, K^{+}, Ca^{2+}, Mg^{2+},SO_4^{2-}, CO_3^{2-}, NO_3^{-}, Cl^{-}, and sub-mM level HPO_4^{2-}. The recorded peak area were compared with that of As(V) ion only.

2.4 *Operando SERS monitoring of catalyzed reaction.*

To in-situ monitor Pd catalyzed KBH_4 reduction of *p*-NTP to *p*-ATP, the deposited Ag@Pd NPF was immersed in 0.1 mM *p*-NTP ethanol solution for 30 min to form a SAM of p-NTP on the NPF surface. After washed by copious of ethanol and air-dried, the slide was fixed onto a lab-made reactor, with NWs film exposed to the inter of the reactor (more details can be find in *J Phys Chem Lett* **2014**, *5*, 969.).[2] The reactor was placed on the XYZ stage of the Raman microscope. The Raman spectra was acquired in successive mode in the situ of the film, the 785 nm laser power was maintained at 0.1mW, the integration time was 0.5 s, and the overall time was 0.665s per spectra. After a stable spectrum was acquired, 0.2 mM KBH_4 aqueous solution was injected the reactor to initiate the reaction. The reaction rate constant K can be calculated by equitation (1),

$$\mathrm{Ln}C_t/C_0=\mathrm{Ln}(I_{1340\,(t)}/I_{1340\,(t=0)})=kt+b \qquad (1)$$

2.5 Characterization.

The UV-Vis-NIR absorbance property of the synthesized NWs was characterized by a Shimadzu 3600 UV-Vis-NIR spectrometry, and the acquired spectra were normalized by the concentration of Ag NWs. The crystal structure was determined by X-ray diffraction (XRD) analysis, which was performed with an X' pert PRO instrument (PANalytical) using Cu Kα radiation (λ = 0.15418 nm). The morphology of

NWs was observed by a high resolution transmission electron microscopy (HRTEM) and a field emission scanning electron microscopy (FESEM). HRTEM analysis was fulfilled on a Tecnai G2 F-20 (FEI) HRTEM, the species were prepared by loading 5 μL aliquots of the aqueous sample onto ultra-thin amorphous carbon film-coated copper grid sample holders, and excess water was removed quickly with filter paper. FESEM was conducted on a SU-8020 (Hitachi). If not stated elsewhere, all Raman experiments were performed on a RenishawInVia Raman microscope equipped with 532, 633 and 785 nm Laser lines as the excitation source, and the Raman band of a silicon wafer at 520 cm^{-1} was used to calibrate the spectrometer.

3. Results and Discussion

3.1 Formation mechanism of Ag NWs and Ag NPF.

Just like the synthesis of Au, Pd or Pt ultrathin nanowires (NWs),[1]TX-114 may work both as stabilizer and structure-director in the synthesize of Ag NWs. After stirring the mixture of 25 mg TX-114 and 47 ml 2.0 mM $AgNO_3$ in an ice bath for 30.0 min, a fresh prepared ice-cold KBH_4 solution was quickly injected to them with a final concentration of 12.0 mM. The colorless $AgNO_3$ immediately changed into bright-yellow and then black or dark-green, indicating the formation of Ag nanoclusters and then Ag NWs. Please note that if the concentration of $AgNO_3$ is lower than 2.0 mM, c.a., 1.0 mM, no Ag NWsform, and the solution is always yellow or yellow-red, very stable and no Ag NPF can be formed. Meanwhile, the concentration of KBH_4 should be higher than 8.0 mM, otherwise no Ag NPF form We believe that at low concentration of $AgNO_3$, all facets of the formed Ag nanoparticles/nanoclusters are stabilized by TX-114, thus no clean {111} facet is available for the oriented attachment process. On the other hand, compared with other noble metal like Au, Pd and Pt, for the lack of unoccupied *d-orbit*, the π-d interaction between TX-114 and Ag atoms is very weak, that is why the morphology of Ag NWs is less uniform than that of Au, Pd or Pt ultrathin NWs. Meanwhile, for the low interaction between TX-114 and Ag NWs, even in the absence of other ions that compete binding site with TX-114,[3] part of absorbed TX-114 will gradually desorbed from Ag NWs and induced the sedimentation/self-organization of Ag NWs in Ag NPF. In fact, if we add halide ions Cl^- or Br^-, the sedimentation process of Ag NWs will be largely accelerated.

It is deserved to note that although under the optimized synthesis condition, the majority of the formed Ag nanoojective are Ag NWs, some Ag NPs that did not incorporated into Ag NWs still existed in the dispersion, and these Ag NPs can also precipitate on Ag NPF or absorb on Fe oxides.

3.2 Characterization of the formed Fe oxides NSs.

For the propose of enriching As(III)/As(V) ion from water sample, we tried to add $FeCl_3$ into the fresh synthesized Ag NWs for in-situ generation of Fe oxides and co-precipitate them into Ag NPF. As we expected, transparent nanosheets (NSs) with area reached micrometer-size formed (Figure S4A, D), while scanning transmission electron microscope (STEM) image showed that some nanoparticles with much higher brightness than NSs are also present, and EDS analysis reveal that these nanoparticles are Ag nanoparticles that are not integrated into Ag NWs (Figure S4B). HRTEM images show a lattice spacing of 0.48 nm, which can be assigned as the {111} facet of γ-Fe_2O_3 (Figure S4C). The chemical composition was further probed by XPS (Figure S4E1, 2). The core-level XPS spectra of Fe show a binding energy of Fe $2p_{3/2}$ and Fe $2p_{1/2}$ electrons at 711.2 and 724.4 eV, as well as two satellite peaks at 719.2 and 732.4 eV, a result of charge-transfer screening, Indicating the main component is Fe^{3+}.[4] Cl 2p electrons display double peaks located at 197.8 and 199.4 eV, which can be assigned to the characteristic doublets of Cl $2p_{3/2}$ and Cl $2p_{1/2}$, and Ag also in its metallic state with Ag 3d electrons located at peaks at 368.2 and 374.2 eV (Figure 4E2).[5] Besides demonstrating the addition of $FeCl_3$ has neglectable effect on the chemical state of Ag, the above results also infer the presence of γ-Fe_2O_3 in

the formed nanostructure. However, not Fe oxide associated peak were detected in XRD experiment (Figure S7), which can be explained by the low sensitivity and small amount of such material in the fabricated nanocomposites, this notion is conclusive enough.

We further characterized the formed Fe oxides by enhanced Raman spectra (Figure S5). Under the excitation of 532 nm Laser, three broad peaks were observed at 375, 670 and 1320 cm^{-1}, these peaks were assigned to γ-Fe_2O_3.[6] However, the relative intensity of these peaks largely decreased under the excitation of 633 nm Laser, and almost attenuated as small shoulders under the excitation of 785 nm Laser. This deference in the relative Raman intensity for γ-Fe_2O_3 under the excitation of different Laser is reasonable for inorganic nanostructure like γ-Fe_2O_3, whose Raman intensity is proportional to the fourth power of the Scattered light frequency.[7] Besides the peaks of γ-Fe_2O_3, two strong peaks that located at 547 and 233 cm^{-1} are also observed, both under the excitation of visible and near infra Laser. A plausible assignment for the peak at 233 cm^{-1} is the Raman peak of AgCl, as this peak is also observed in Ag NPF formed in the presence of Cl^-, but not on Ag NPF alone.[8] The assignment of the peak at 547 cm^{-1} is very challenge, we hypothesize that it is associated with surface oxides/hydroxide of Ag like AgO, Ag_2O or AgOHon Ag NPF surface, as the Raman peak of most metal oxides/hydroxides located at this area. If this peak do associated with AgOH, the interference of high concentration of Cl^- (1.0 mM or above) on the SERS detection of As ion would be reasonable. As a small amount of As ion may be absorbed on Ag surface through Ag^+ in AgOH, while in the presence of high concentration of Cl^-, those sites will be taken up by Cl^-. Anyway, from our experiment result, the interference from Cl^- was far less serious than that of HPO_4^{2-}, thus demonstrating the corporation between γ-Fe_2O_3 NSs and Ag NPF, the γ-Fe_2O_3 NSs adsorb As ion and Ag NPF offers an electromagnetic field (EM) for enhancing the Raman signal, is the main mechanism for the SERS detection of As ion on Ag NPF-γ-Fe_2O_3 NSs.

It should be noted that all spectra were acquired at the same location of the sample in the order of 532, 633 and 785 nm, and the laser power is very low (0.1 mW or lower), so it is possibility that the detected γ-Fe_2O_3 is formed from photo-transform of other Fe oxide is very low.

In one word, both electron microscopic and spectroscopic results support the notion that the majority of synthesized Fe oxide in Ag NPF-Fe oxide nanocomposite is γ-Fe_2O_3. According to our unpublished work,[9] in the presence of proper amount of TX-114, reducing $FeCl_3$ with KBH_4 and aging the result solution in aerobic condition will give birth to γ-Fe_2O_3 NSs, or γ-Fe_2O_3 NSs is produced by the oxidation of Fe(0) nanoclusters and oriented attachment of the resulting Fe oxide. However, for the complexity of Fe oxides, and Fe(0) oxidation process, the possibility of other Fe oxides like green rust still coexists with γ-Fe_2O_3 canbe exclude at present.

Of noted is that the color of fabricated nanostructure are dark-green for Ag NWs dispersion, black for Ag@Pd NPF, grey green for Ag NPF, and black green for Ag-Fe oxide. (Figure S2) and the color of Ag NPF-oxides was dark green before dry, and then become light-green after dry. So the color of green may not be from green rust but Ag NWs themselves. We feel sorry for the mistake we made in the description of the production of the iron oxide/silver nanocomposition, and this information has been corrected.

3.3 Adding Na_2PdCl_4 and $FeCl_3$ into the fresh synthesized Ag NWs dispersion.

Compared with other Pd precursor like $Pd(NO_3)_2$, Na_2PdCl_4 is easy coated on Ag surface as Pd overlayer (data not shown). One possible reason is the strong interaction between Cl^- and Pd^{2+} ion slow down the reduction rate of Pd^{2+}, and lowered the saturation degree of Pd atoms, thus the formation of Pd nucleus is largely suppressed and the deposition of Pd atoms on Ag is promoted. On the other hand, the added Cl^- not result in the formation of AgCl, at least the amount of formed AgCl is very low, as no peak of AgCl can be identified in the corresponding XRD pattern (Figure S7). The absence of AgCl indicates no direct reaction between Ag and Pd^{2+} or Fe^{3+}, as Cl^- alone cannot react with Ag NPF to form AgCl.[10]Besides the absence of AgCl in the XRD pattern, no peak associated with Pd or γ-Fe_2O_3 is observed in the XRD result ether. This result can be attributed to their low amount and low sensitivity in XRD detection.

Meanwhile, if directly injecting Na_2PdCl_4 or $FeCl_3$ into $AgNO_3$ solution, the solution quickly change from colorless into milk-like white, and TEM analysis reveal that abundant AgCl crystal, both in the form of nanocube and nanobars, are formed (Figure S8).

3.4 Calculation the SERS EF of Ag NPF

To quantify the SERS performance of Ag NPFs, we calculated SERS enhancement factor (EF) using the following equation:

$$EF = \frac{I_{SERS} * P_{NR} * T_{NR} * n_{NR}}{I_{NR} * P_{SERS} * T_{SERS} * n_{SERS}}$$

Here, I_{SERS}, I_{NR}, P_{SERS}, P_{NR}, T_{SERS}, T_{NR}, n_{SERS} and $n_{NR}$are referred as the Raman intensity (I), the laser power (P), the integration time (T) of the normal (NR) and enhanced Raman (SERS), respectively. The intensity is taken at the Raman peak at 1619 cm^{-1}. The n_{NR} and I_{NR} are obtained directly using solid crystal CV molecules placing on the silicon substrate. n_{NR} of CV molecules is calculated by $N_{av}(\rho V_{laser}/M)$,[11] in which Nav is the Avogadro number, V_{laser} is the focal (or probe) volume of the laser illumination, M is the molecular weight of SERS molecules (407.98 $gmol^{-1}$ for CV), and ρ is the density of the single crystal (1.19 gcm^{-3} for CV), respectively. $V_{laser}$is estimated by (1/3) $\pi R^3 h$, in which R is the radius (~ 0.70 μm), and h is the depth of (~20 μm) of the laser. The value of n_{NR} is calculated to be 1.43×10^{10}. While $n_{SERS}=C_{probe}V_{probe}S_{spot}/S_{substrate}$, where C_{probe} is the concentration of CV molecule, which is ranged from 10^{-6} to 10^{-12} M, V probe is 10 μL or 10^5 L, Sspot is about 1 μm^2 and $S_{substrate}$ is the area of substrate (1 cm^2). The measured I_{Ref} is 4700, 1100 and 1400 counts $mW^{-1}S^{-1}$ under the excitation of 532, 633 and 785 nm Laser, respectively. Thereby the calculated EF is $5.52\pm2.43\times10^8$, $1.27\pm0.51\times10^{10}$, and $8.93\pm3.72\times10^6$ under the excitation of 532, 633 and 785 nm Laser, respectively (Figure S10).

The large enhancement factor, especially for that under the excitation of 532 and 633 nm Laser, where the enhancement factor is large than 10^8, is sufficient for single molecule detection (SMD).[12]For the demonstration of SMD, 10 μL 10^{-13} M CV were loaded on 1.0 cm^2 Ag NPF, which resulted in an average probe molecule density of 0.06 μm^2, and 1000 spectra were recorded with a step size of

1.0×1.0 μm^2. By analysis the Raman intensity at 1619 cm^{-1}, 25 spectra are identified as the SERS spectra of CV, and this was supported by comparing these spectra with the standard one (Figure S11).

3.5 The effect of Pd and γ-Fe_2O_3 NSs on the SERS performance of Ag NPF.

As the presence of Pd, especially when Pd overlayer on Ag surface, may damp the SPR properties of Ag, thus the SERS activity of Ag@Pd NPFs are not as good as that of Ag NPF alone. This speculation is supported by the recorded SERS spectra of CV on Au@Pd NPF (8.0 %) (Figure S12), where the detection limit is in the range of 10^{-9}-10^{-8} M, much lower than that of Ag NPF. While, in the case of Ag NPF-γ-Fe_2O_3 NSs that were just doped Ag NPF, the SERS sensitivity of CV isless effected and the limit of detection is in the range of 10^{-10} to 10^{-9}M (Figure S13).

3.6 Demonstration of the existence of AgCl on Ag surface in Ag-NPF-γ-Fe_2O_3 NSs.

The existence of AgCl on Ag surface in Ag-NPF-γ-Fe_2O_3 NSs is further verified by the altered SERS performance. To exclude the negative effect of γ-Fe_2O_3 NSs on the SERS activity of Ag NPF, Ag NPF prepared in the presence of equal amount of Cl^- (0.6 mM) was used (denoted as Ag NPF(Cl)) as control. Three Raman probes whose affinity for Ag in the order of As(V) ion<SCN-<ABT were employed. Before SERS analysis, both Ag NPF (Cl) and Ag NPF were placed into 5 ml of probe molecule with changing concentration for the adsorption of these molecules. 30 min later, the NPFs was rinsed with copious water/ethanol for 3 times to remove the unbounded probe molecules (Figure 15).

3.7 Attribution of the Raman peaks at ~2110 and ~2000 cm^{-1}.

There are three possible atomic geometries of Pd atoms on Ag NPF surface, *i.e.* isolated Pd atoms, Pd ensemble on Ag surface and Pd NWs anchored on Ag NPF. Meanwhile, there are three possible binding configurations of 2,6-DMPI molecule on Pd, *i.e.* atop-binding and bridged/three fold hollow site binding, which correspond to the Raman peak at ~2110 and ~2000 cm^{-1}, respectively. As the peak at ~2000 cm^{-1} is very low before the Pd coverage reaching 1.0%, coincidentally, not Pd NWs is observed in FESEM images (Figure S6). Thus, it is very certain to ascribe the peak at ~2110 cm^{-1} to Pd layer, while the peak at ~2000 cm^{-1}to Pd NWs/branches.

4. Figures

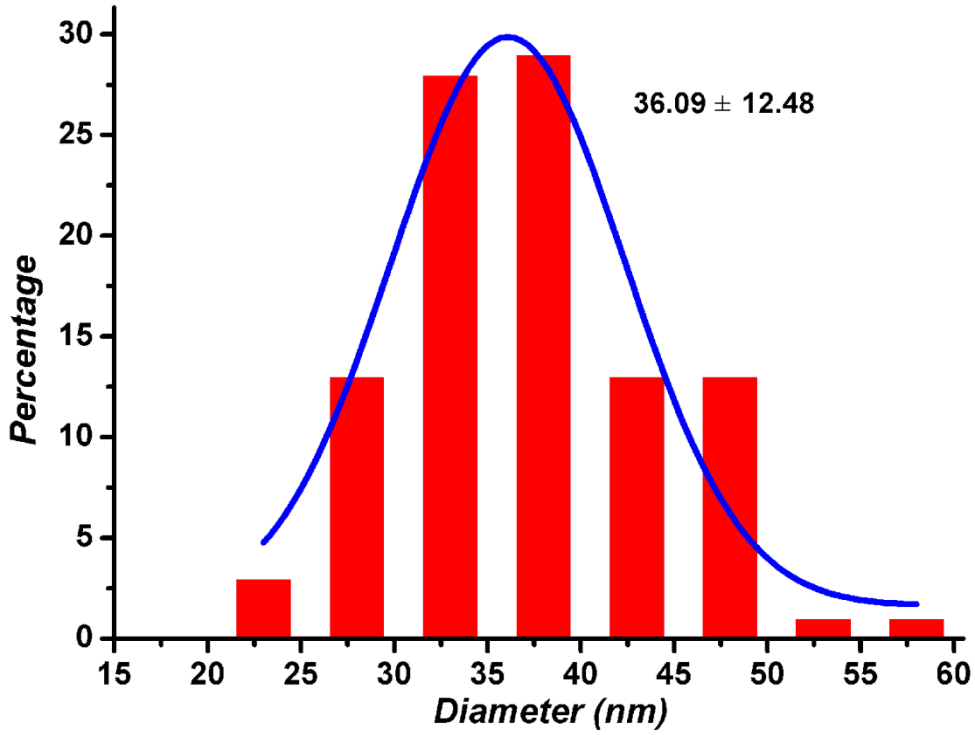

Figure S1. The distribution of the diameter of Ag ligament in Ag NPF, Gauss fitting shows that the average size is 36.09±12.48 nm, and this value match well with XRD result (about 32 nm).

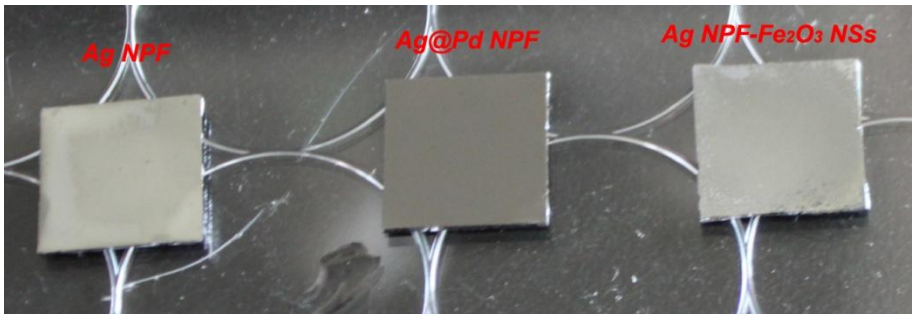

Figure S2. Photograph of the fabricated Ag NPF, Ag@Pd NPF and Ag NPF-γ-Fe_2O_3 NSs hybird nanocomposite. The color of Ag NPF is very similar to that of Ag metal, while for the damping effect of Pd to the optical property of Ag, the Ag@Pd NPF displays a light black color, while for Ag NPF-γ-Fe_2O_3 NSs, may be for the surpressed further interconnection of Ag NWs, its color is very similar to that of Ag NWs.

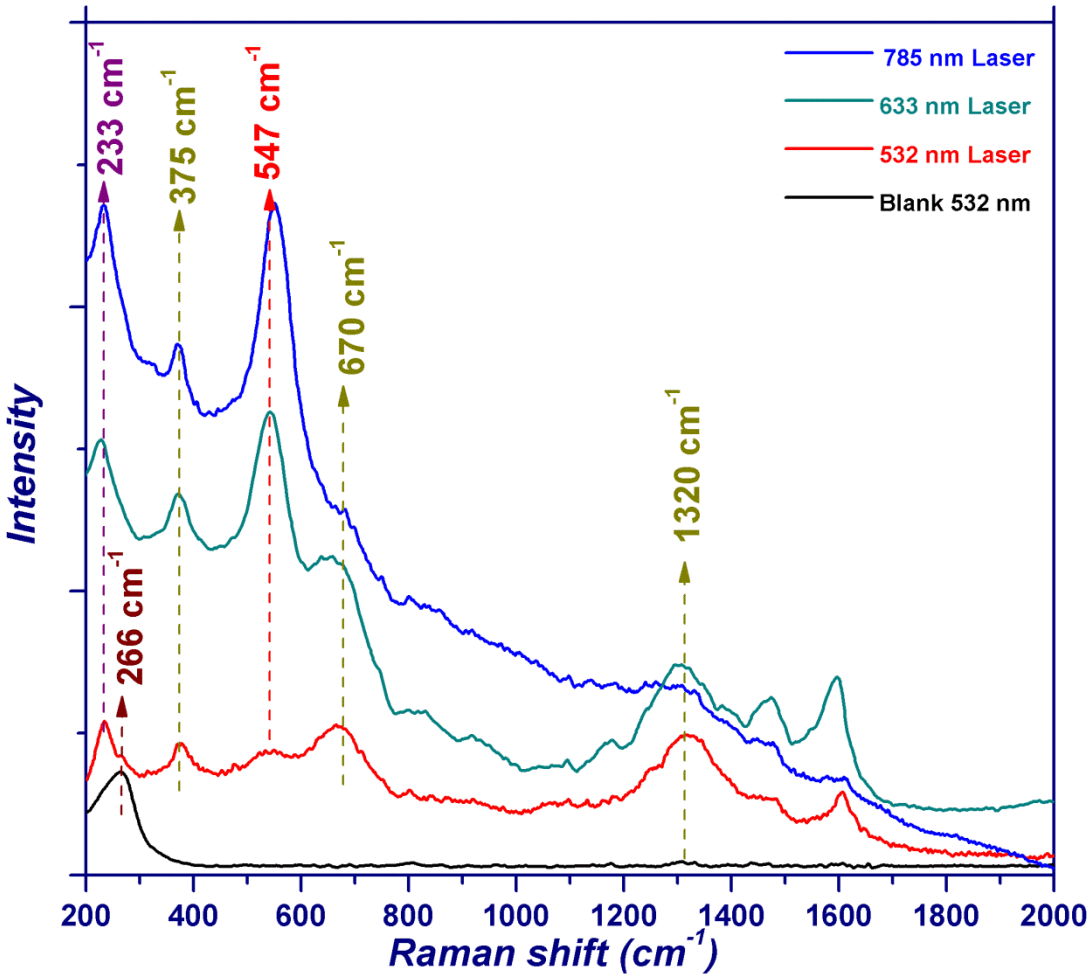

Figure S3. The enhanced Raman spectra of Fe oxide NSs under the excitation of 532, 633 and 785 nm Laser. The spectra of Ag NPF under the excitation of 532 nm Laser is also present for comparison.

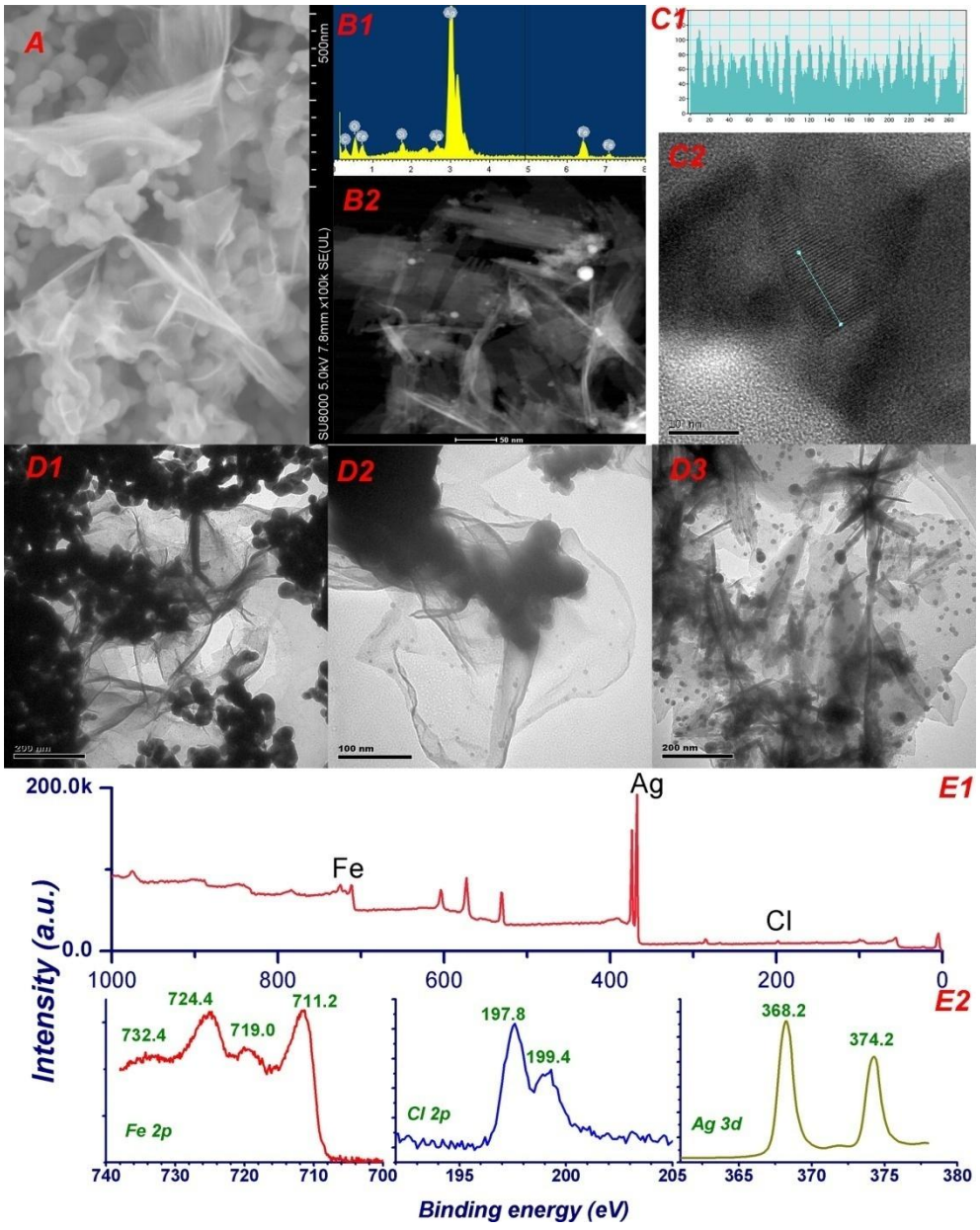

Figure S4. Characterization of Ag NPF-Fe oxide NSs by (A) FESEM, (B)STEM/EDS, (C) HRTEM, and (D) Low-magnified TEM, and probe the chemical composition and the valence state of Fe, Ag and Cl XPS (E). The EDS spectrum in B1 was acquired from the nanoparticles (bright particle in B2). The marked area by green line in C2 was highlight in C1

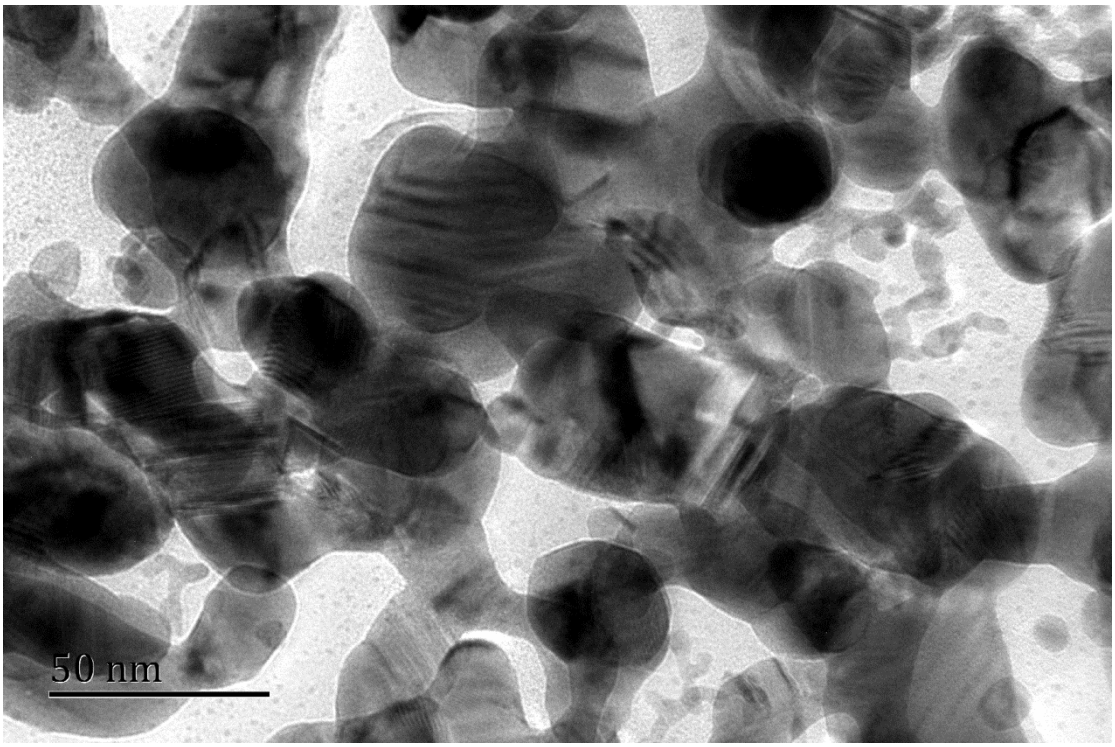

Figure S5. High-magnified TEM image of Ag@Pd shows the existence of alternate bright and dark Moire' patterns that due to the superposition of two misfit crystalline lattices.

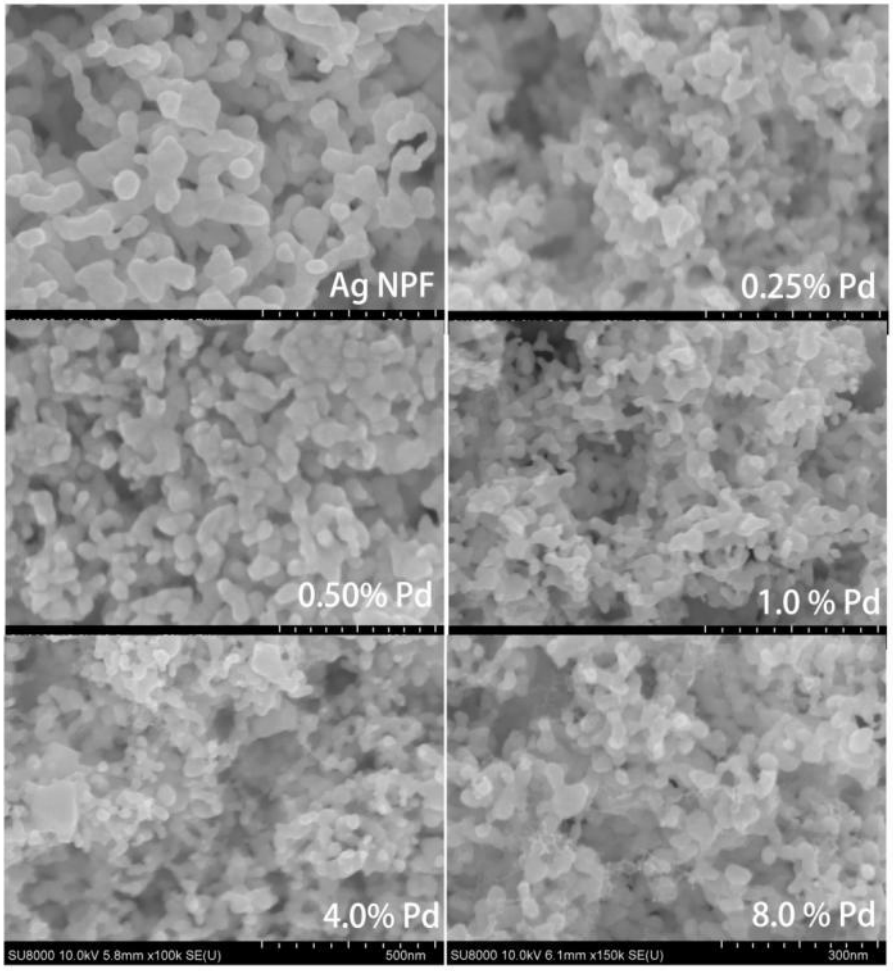

Figure S6. Field emission SEM images of Ag@Pd NPF with changing Pd amount.

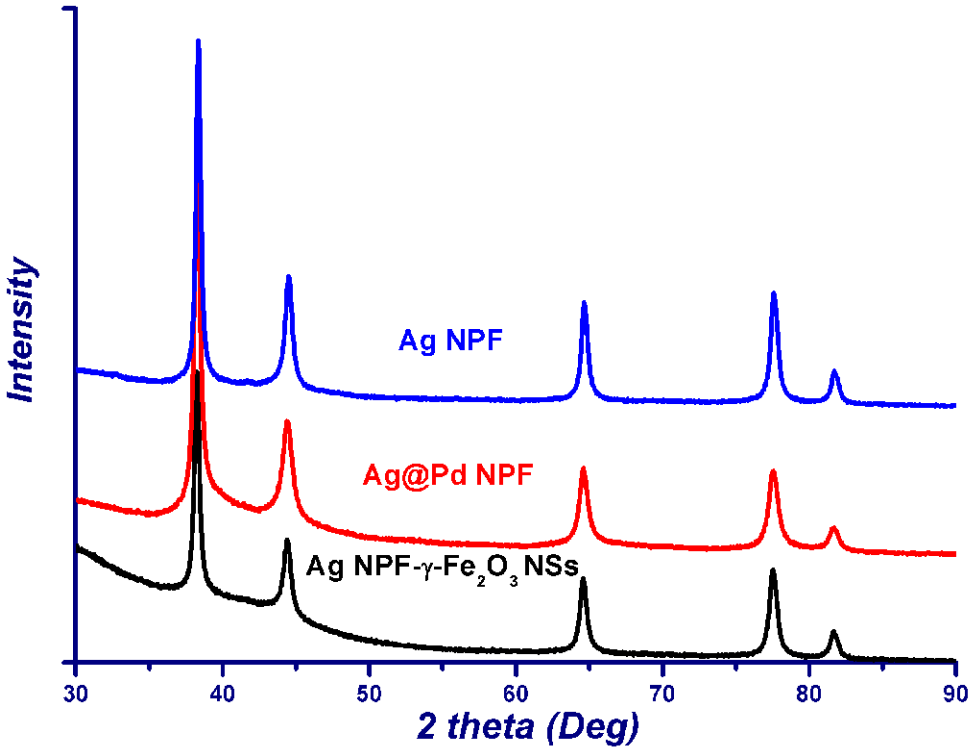

Figure S7. XRD pattern of Ag NPF prepared in the presence of 0.6 mM Cl^-, Ag@Pd NPF and Ag NPF-γ-Fe_2O_3 NSs. No peak of AgCl and γ-Fe_2O_3 were detected.

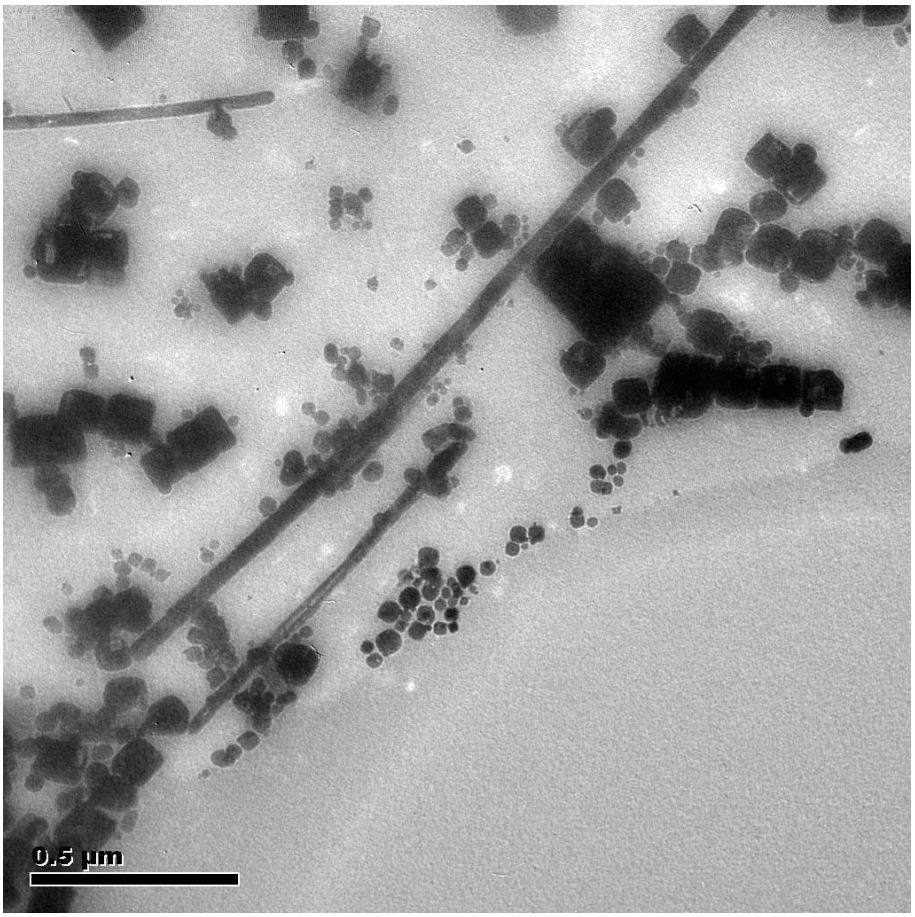

Figure S8. TEM image shows the formation of AgCl nanocubes and nanobars by injecting $FeCl_3$ into $AgNO_3$ solution.

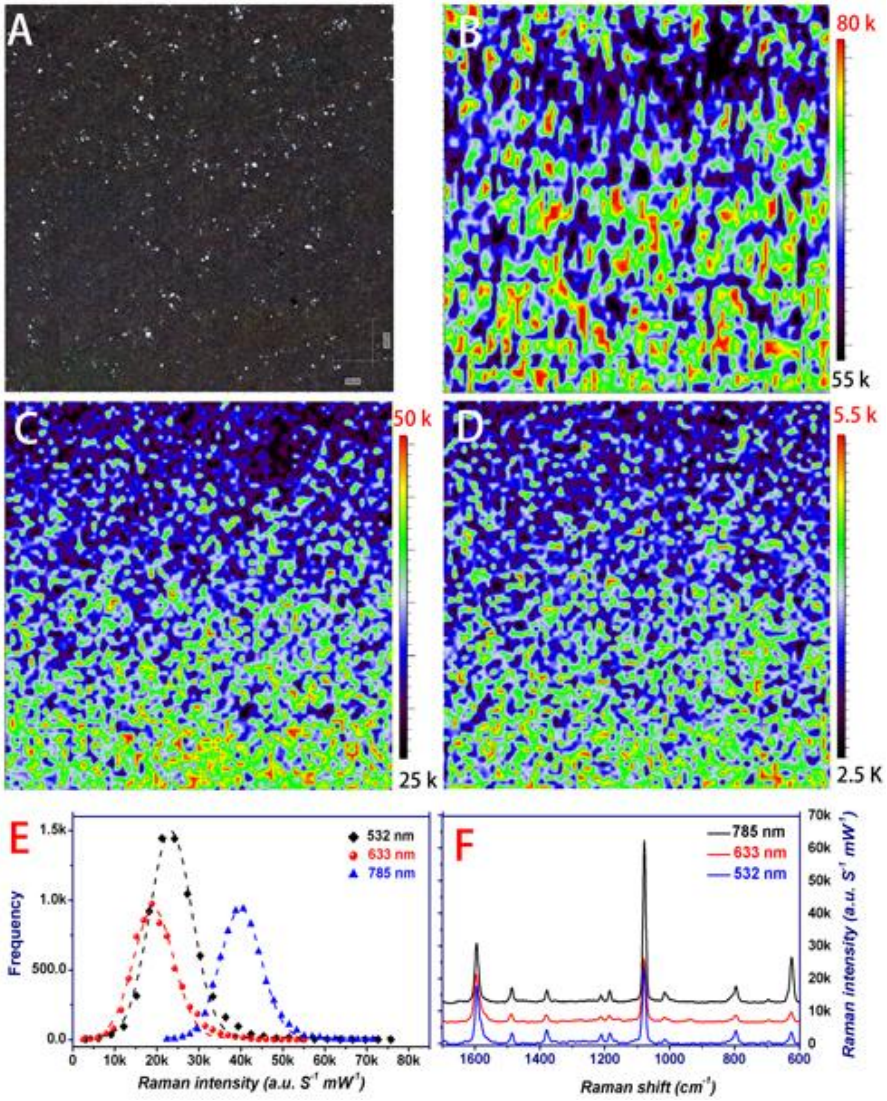

Figure S9. (A) White light image of a Ag NPF (400μm × 400μm). (B-D) SERS intensity mapping at 1077 cm^{-1} corresponding to the area shown in (A) under the excitation of 785 (~0.2 × 10^6mW cm^{-2}), 633 (~1.0× 10^6mW cm^{-2}) and 532(~1.0 × 10^5 mW cm^{-2}) nm Laser. (E) Distributions of the frequencies of occurrence of the Raman intensity at 1077 cm^{-1} in the 6561 spectra measured. (F) Representative SERS spectra of the probe molecule BP under the excitation of different Laser.

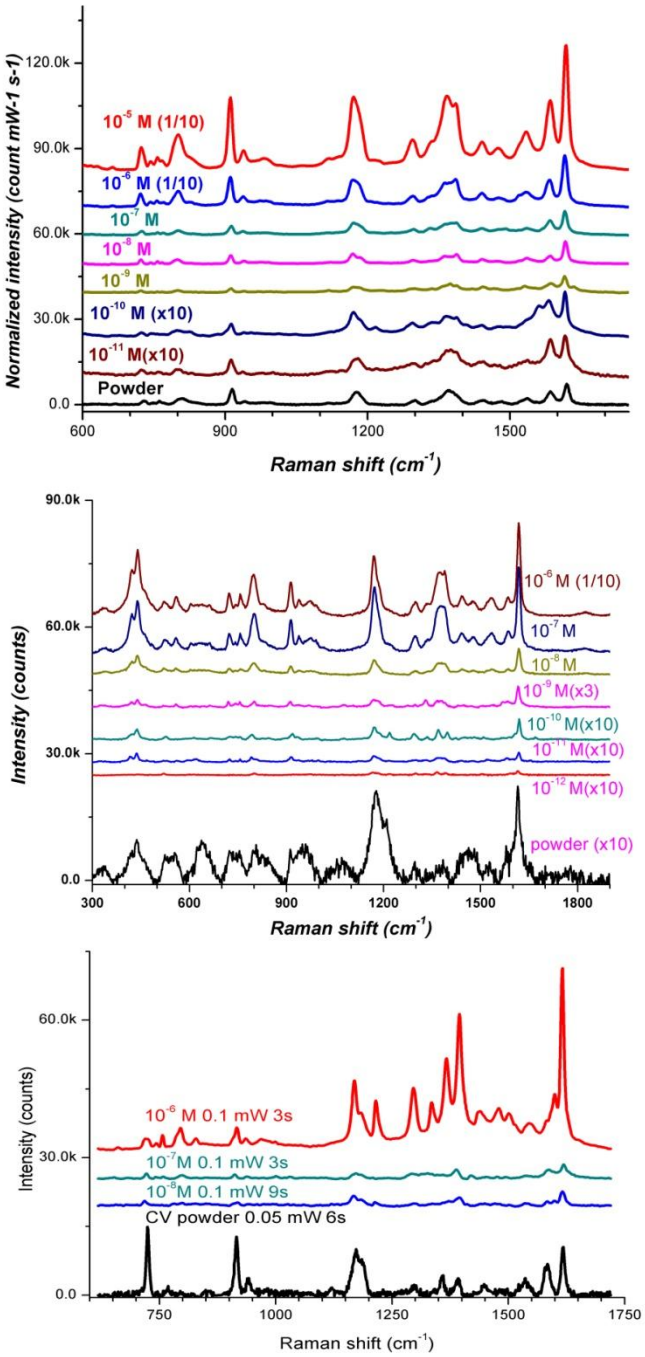

Figure S10. SERS spectra of CV on Ag NPF, from upper to lower: 532 nm Laser, 633 nm Laser and 785 nm Laser.

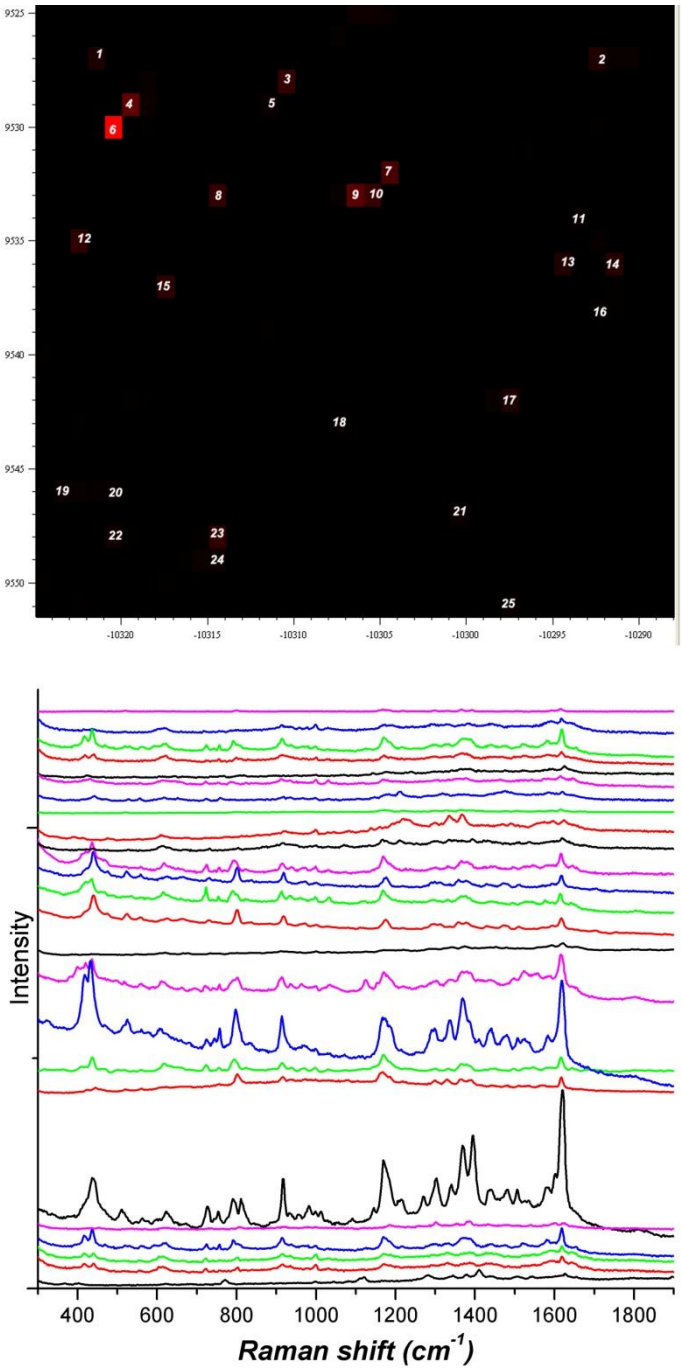

Figure S11. Demonstration of Single molecule detection of CV on Ag NPF, the average amount of CV molecule is 0.06 μm^{-2} (10 μL of 10^{-13}M ethanol solution of CV on 1.0 cm2 Ag NPF), and 25 out of 1000 spectra were identified.

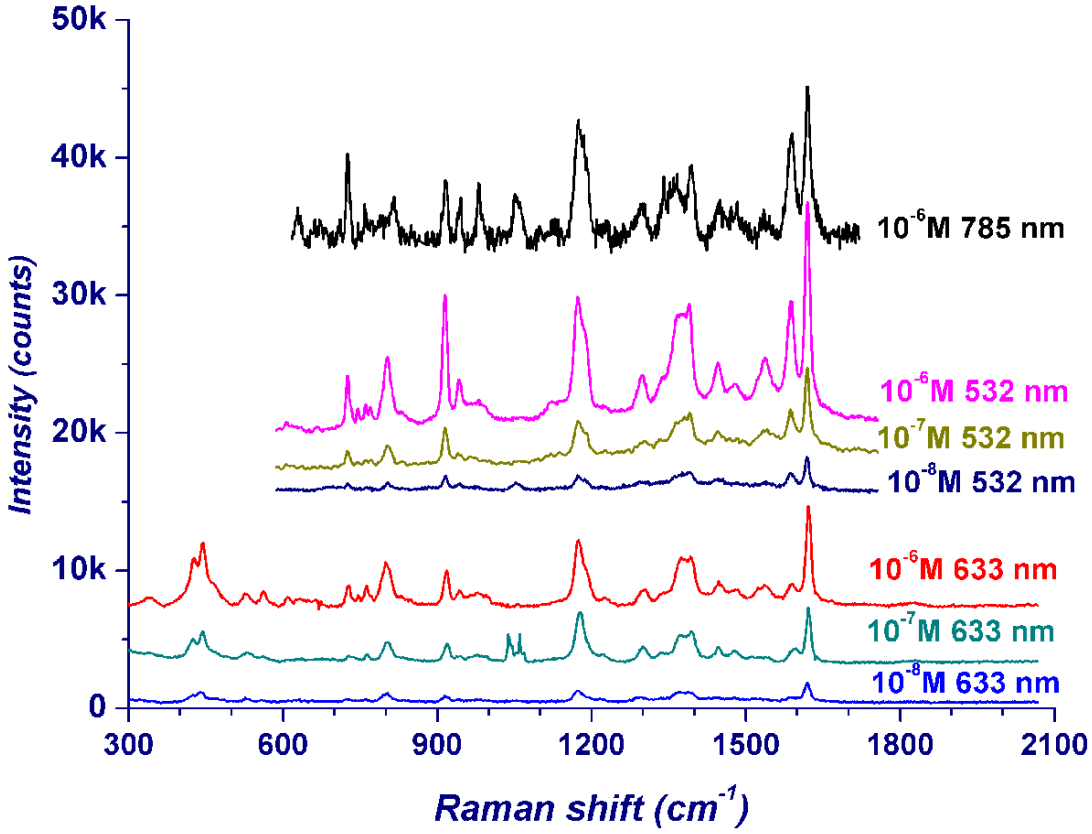

Figure S12. Effect of Pd layer on the SERS performance of Ag NPF: SERS spectra of CV on Ag@Pd NPF (the amount of Pd is 8.0%) under the excitation of different Laser.

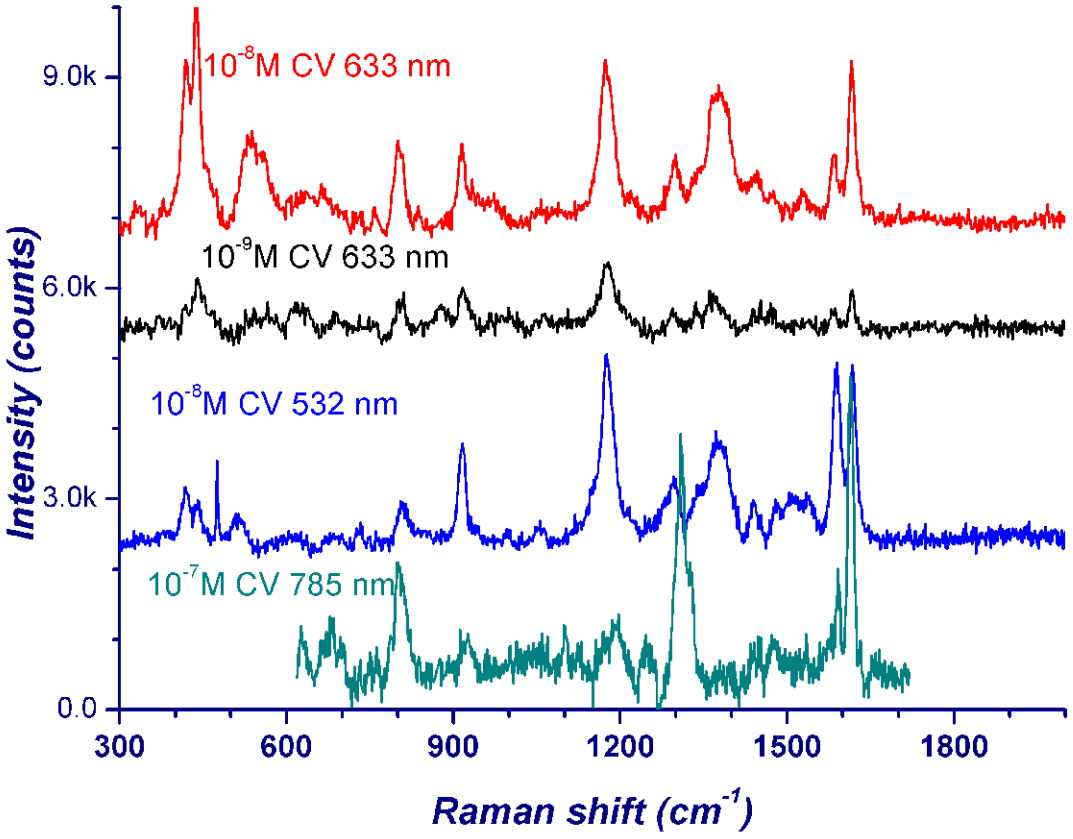

Figure S13. Effect of γ-Fe_2O_3 NSs on SERS performance of Ag NPF: the SERS spectra of CV on Ag NPF-γ-Fe_2O_3 NSs (the amount of Pd is 8.0%) under the excitation of different Laser.

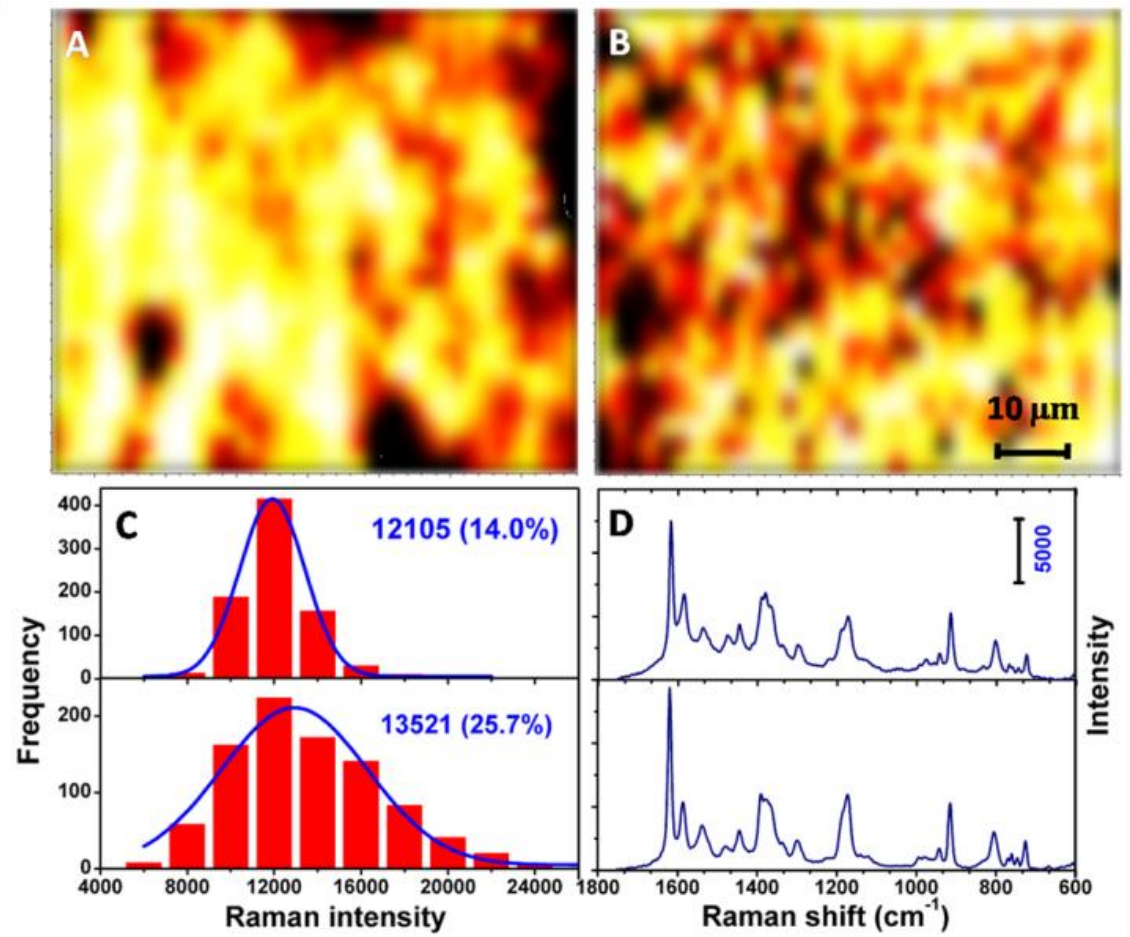

Figure S14. Large area mapping shown the presence of AgCl has neglectable effect on the SERS activity of Ag NPF. (A, B) SERS intensity mapping on Ag NPF and Ag@AgCl NPF, and (C, D) the corresponding intensity distribution and representative Raman spectra of 10^{-7} M CV on Ag/AgCl (upper) and Ag NPF (lower).

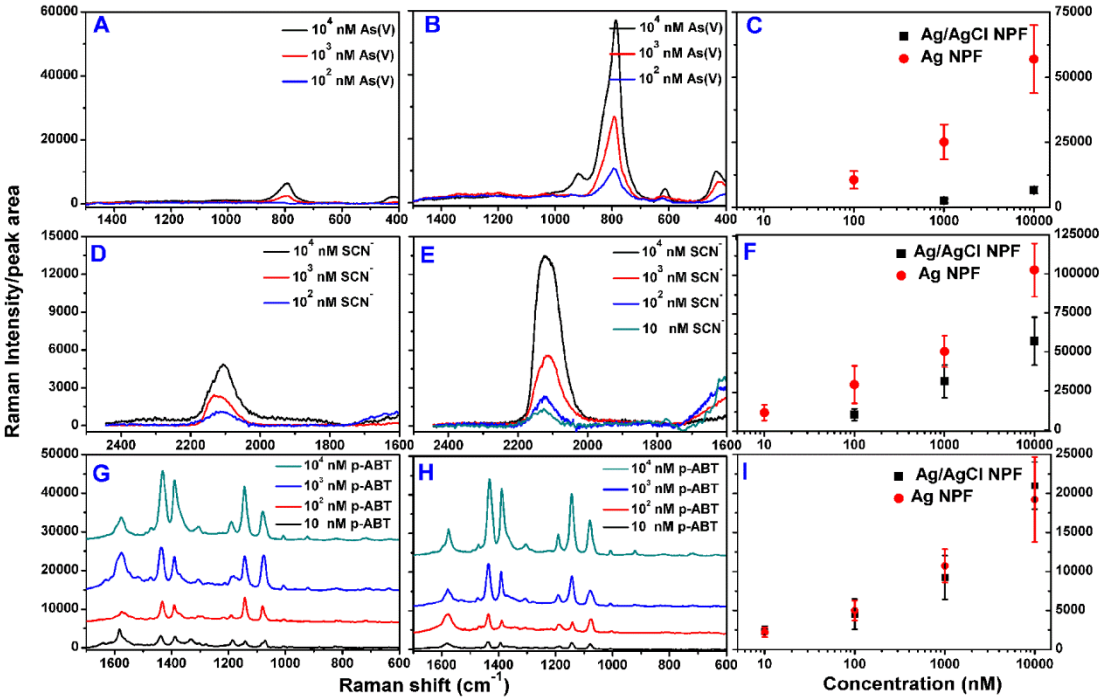

Figure S15. Demonstration of the presence of AgCl layer on Ag NPF formed in the presence of 0.3 mM Cl^-. (A-C) In the presence of Cl^-, As ion is only weakly adsorbed on Ag NPF and results much lower sensitivity in detecting As ion than Ag NPF prepared without Cl^-, (D-E) Only part of Cl^- in AgCl can be replaced by SCN^- and reflected in improved relative sensitivity, (G-I) due to the high affinity of –SH and –NH2 with Ag, no significant difference were observed in the SERS detection of ABT on Ag NPF prepared in the presence of absence of Cl^-.

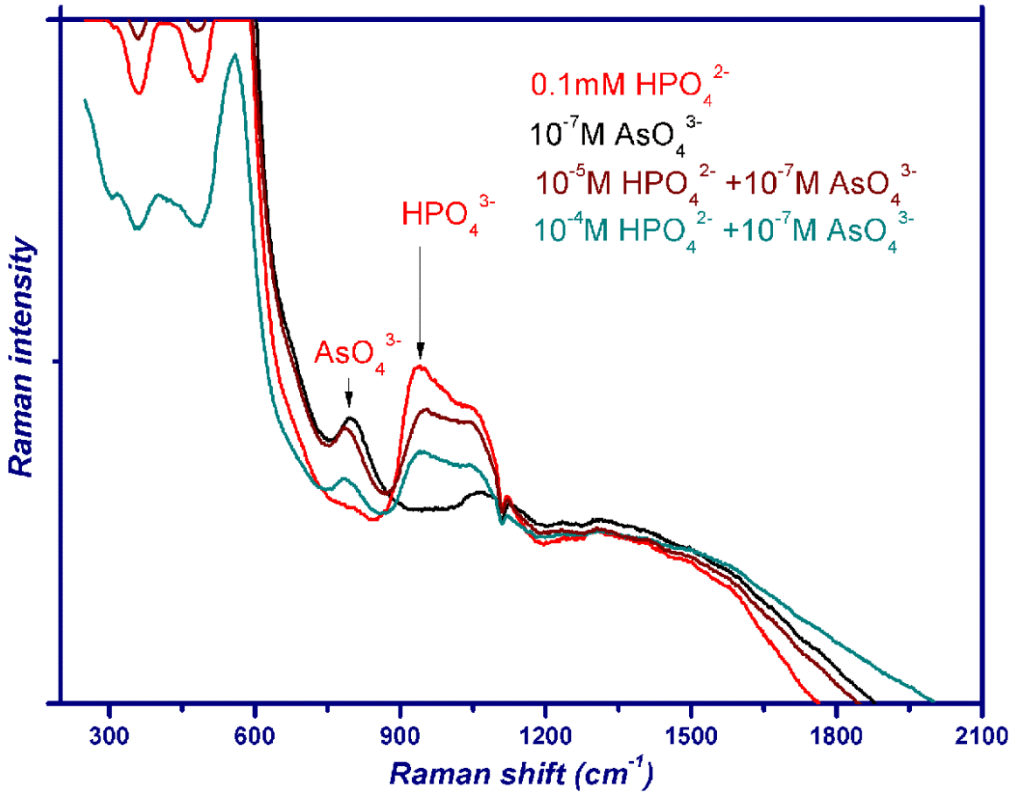

Figure S16. Representative SERS spectra of As(V) and/or HPO_4^{2-} ion captured on Ag NPF-γ-Fe_2O_3 NSs.

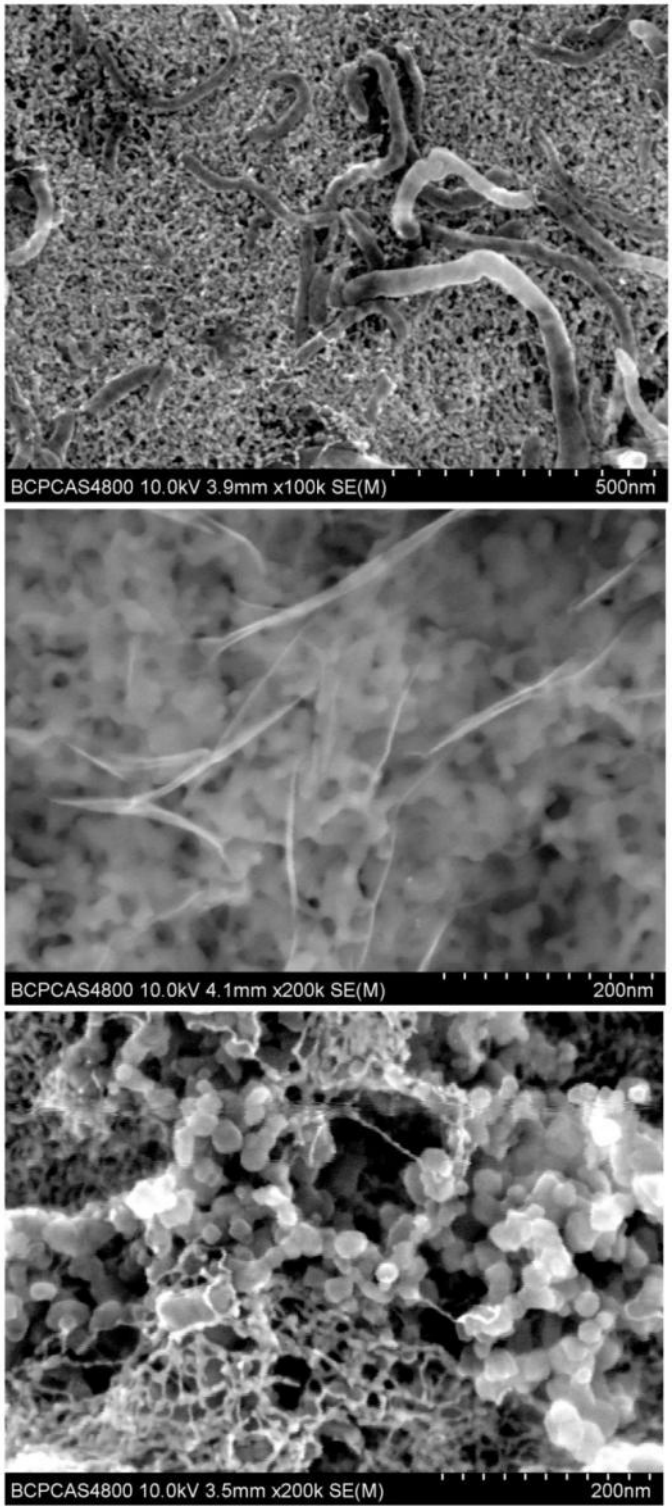

Figure S17. FESEM images of multi-wall carbon nanotube, reduced Graphene oxide and TiO_2 nanoparticles (P25) dipped Au NPF.

5. Reference

(1) Liu, R.; Liu, J. F.; Jiang, G. B. *Chem Commun***2010**, *46*, 7010.

(2) Liu, R.; Liu, J. F.; Zhang, Z. M.; Zhang, L. Q.; Sun, J. F.; Sun, M. T.; Jiang, G. B. *J Phys Chem Lett***2014**, *5*, 969.

(3) Liu, R.; Liu, J. F.; Yu, S. J.; Liu, Q. A.; Jiang, G. B. *Chem Commun***2011**, *47*, 1613.

(4) Fujii, T.; de Groot, F. M. F.; Sawatzky, G. A.; Voogt, F. C.; Hibma, T.; Okada, K. *Phys Rev B***1999**, *59*, 3195.

(5) Dong, R. F.; Tian, B. Z.; Zeng, C. Y.; Li, T. Y.; Wang, T. T.; Zhang, J. L. *J Phys Chem C***2013**, *117*, 213.

(6) Colomban, P.; Cherifi, S.; Despert, G. *J Raman Spectrosc***2008**, *39*, 881.

(7) Fan, F. T.; Feng, Z. C.; Li, C. *Chem Soc Rev***2010**, *39*, 4794.

(8) Grzelczak, M.; Sanchez-Iglesias, A.; Rodriguez-Gonzalez, B.; Alvarez-Puebla, R.; Perez-Juste, J.; Liz-Marzan, L. M. *Adv Funct Mater***2008**, *18*, 3780.

(9) Liu, R.; Liu, J. F.; Zhang, L. Q.; Sun, J. F.; Zhang, Z. M.; Jiang, G. B. *submited*.

(10) Li, Y. Y.; Ding, Y. *J Phys Chem C***2010**, *114*, 3175.

(11) Cho, W. J.; Kim, Y.; Kim, J. K. *Acs Nano***2011**, *6*, 249.

(12) Patra, P. P.; Kumar, G. V. P. *J Phys Chem Lett***2013**, *4*, 1167.